J. Mater. Sci. 53 (2018) 1024–1034

DOI: 10.1007/s10853-017-1609-1

https://doi.org/10.1007/s10853-017-1609-1

Magnetic, optical, dielectric, and sintering properties of nano-crystalline $BaFe_{0.5}Nb_{0.5}O_3$ synthesized by a polymerization method

Roberto Köferstein*, Florian Oehler, and Stefan G. Ebbinghaus

Institute of Chemistry, Martin Luther University Halle-Wittenberg,

Kurt-Mothes-Strasse 2, 06120 Halle, Germany.

J Mater Sci

Ceramics

Magnetic, optical, dielectric, and sintering properties of nano-crystalline $BaFe_{0.5}Nb_{0.5}O_3$ synthesized by a polymerization method

Roberto Köferstein[1,*], Florian Oehler[1], and Stefan G. Ebbinghaus[1]

[1] Institute of Chemistry, Martin Luther University Halle-Wittenberg, Kurt-Mothes-Strasse 2, 06120 Halle, Germany

Received: 3 July 2017
Accepted: 18 September 2017

ABSTRACT

A one-pot polymerization method using citric acid and glucose for the synthesis of nano-crystalline $BaFe_{0.5}Nb_{0.5}O_3$ is described. Phase evolution and the development of the crystallite size during decomposition of the (Ba,Fe,Nb)-gel were examined up to 1100 °C. Calcination at 850 °C of the gel leads to a phase-pure nano-crystalline $BaFe_{0.5}Nb_{0.5}O_3$ powder with a crystallite size of 28 nm. The shrinkage of compacted powders starts at 900 °C. Dense ceramic bodies (relative density ≥ 90%) can be obtained either after conventional sintering above 1250 °C for 1 h or after two-step sintering at 1200 °C. Depending on the sintering regime, the ceramics have average grain sizes between 0.3 and 52 µm. The optical band gap of the nano-sized powder is 2.75(4) eV and decreases to 2.59(2) eV after sintering. Magnetic measurements of ceramics reveal a Néel temperature of about 23 K. A weak spontaneous magnetization might be due to the presence of a secondary phase not detectable by XRD. Dielectric measurements show that the permittivity values increase with decreasing frequency and rising temperature. The highest permittivity values of 10.6×10^4 (RT, 1 kHz) were reached after sintering at 1350 °C for 1 h. Tan δ values of all samples show a maximum at 1–2 MHz at RT. The frequency dependence of the impedance can be well described using a single RC-circuit.

Introduction

Perovskite materials with high dielectric constants are of interest for applications in advanced technologies, e.g. memories and sensors [1–3]. $BaFe_{0.5}Nb_{0.5}O_3$ is interesting as an alternative for lead-containing dielectrics like PZT because it shows high dielectric constants over a wide temperature and frequency range [4]. Patel et al. [5] showed that grain boundary effects are probably causal for the high permittivity values, and investigations by Wang et al. [6] suggest an oxygen defect-induced dielectric behaviour. Some authors describe $BaFe_{0.5}Nb_{0.5}O_3$ as a relaxor ferroelectric with monoclinic cell parameters [7–13]. In contrast, structural investigations by

Address correspondence to E-mail: roberto.koeferstein@chemie.uni-halle.de

DOI 10.1007/s10853-017-1609-1

Journal : 10853 - Large 10853 | Dispatch : 20-9-2017 | Pages : 11
Article No. : 1609 | LE | TYPESET
MS Code : JMSC-D-17-04034 | CP | DISK

Tezuka et al. [14] and Galasso and Darby [15] reveal a centrosymmetric cubic space group, and XRD analyses by Bhagat and Prasad [16] point to a centrosymmetric monoclinic unit cell, indicating a non-ferroelectric nature of $BaFe_{0.5}Nb_{0.5}O_3$ [17–19]. In addition to its interesting and not fully understood dielectric properties, $BaFe_{0.5}Nb_{0.5}O_3$ is an antiferromagnet with a Néel temperature of about 25 K [14] and can be used for the catalytic reduction of NO and the oxidation of CO [20]. Recently, Pan et al. [21] and Chung et al. [22] reported on the dry reforming of methane with CO_2 to form syngas in the presence of $BaFe_{0.5}Nb_{0.5}O_3$. Usually, $BaFe_{0.5}Nb_{0.5}O_3$ is synthesized by the conventional mixed-oxide method, resulting into coarse-grained powders, which need high sintering temperatures [11, 12, 14, 17, 23–26]. Additionally, only few wet-chemical synthesis routes have been reported, such as sol–gel and co-precipitate routes [5, 13, 27] as well as a microwave-assisted synthesis [28]. In addition, a nanoscaled $BaFe_{0.5}Nb_{0.5}O_3$ powder via biosynthesis was reported by Jha et al. [29]. Generally, soft-chemistry syntheses lead to fine-grained/nano-sized powders at low reaction temperatures. Using nano-sized powders, the sintering behaviour can be improved, resulting in a reduction in sintering temperatures and soaking times to from ceramics with tuneable grain sizes.

For this purpose, we report on a one-pot Pechini-like polymerization method using citric acid and glucose to synthesize nano-crystalline $BaFe_{0.5}Nb_{0.5}O_3$ at low temperature with an improved sintering activity. Phase evolution and crystallite growth during the calcination process were monitored by XRD. The sintering behaviour of the nano-powder and the microstructure of resulting ceramic bodies were studied. Furthermore, magnetic and dielectric measurements were carried out, and the optical band gaps of the $BaFe_{0.5}Nb_{0.5}O_3$ samples were determined.

Experimental

Material preparation

$NbCl_5$ (0.007 mol, Alfa Aesar, 99%) and 10 g anhydrous citric acid were dissolved in 60 ml 1,2-ethanediol. Heating to about 100 °C led to a clear solution. Afterwards, $Fe(NO_3)_3{\cdot}9H_2O$ (0.007 mol, Merck, ≥ 99%) and barium acetate (0.014 mol, Sigma-Aldrich, ≥ 99%) were added. The resulting clear solution had a volume of about 80 ml and was stirred at about 190 °C until the volume had decreased to 70 ml. 25 g of glucose monohydrate was added under vigorous stirring, and the solution was continuously heated and stirred until it turned to a clear black–brown viscous gel. This (Ba,Fe,Nb)-gel was calcined for 2 h in static air at various temperatures (heating/cooling rate 10 K min^{-1}), leading to $BaFe_{0.5}Nb_{0.5}O_3$ nano-powders.

To obtain ceramic bodies, a $BaFe_{0.5}Nb_{0.5}O_3$ powder calcined at 850 °C for 2 h (rate 1 K min^{-1}) was mixed with 5 wt % of a saturated aqueous polyvinyl alcohol (PVA) solution as pressing aid and uniaxially pressed at about 40 MPa into pellets (green density 2.7 g cm^{-3}). These pellets were placed on a ZrO_2 fibre mat and sintered to ceramic bodies. Two different sintering procedures were used, namely conventional sintering (heating with 5 K min^{-1}, soaking at this temperature for 1 h, cooling with 5 K min^{-1}) and two-step sintering (heating with 20 K min^{-1} to 1300 °C (T_1), then fast cooling with 20 K min^{-1} to 1200 °C (T_2), and soaking at T_2 for 10 h).

Characterization

X-ray powder diffraction patterns using Cu-K_α radiation were collected at room temperature on a *Bruker D8-Advance* diffractometer, equipped with a one-dimensional silicon strip detector (LynxEye™). Crystallite size and the strain parameter were determined from XRD line broadening (integral peak breadth) using the Scherrer and Wilson equation (software suite WinXPOW [30]). For Rietveld refinement, the FullProf software suite was applied [31]. Dilatometric measurements were carried out in flowing synthetic air (50 ml min^{-1}) in a *Setaram* TMA 92-16.18 dilatometer. Simultaneous thermogravimetric (TG) and differential thermoanalytic (DTA) investigations in flowing synthetic air (20 ml min^{-1}) were performed using a *Netzsch* STA 449 system. The TG/DTA measurement of the decomposition of the (Ba,Fe,Nb)-gel was carried out on a sample preheated at 250 °C. The specific surface area (BET) was determined using nitrogen five-point gas physisorption (Nova 1000, Quantachrome Corporation). The equivalent BET particle diameters were calculated assuming a spherical or cubic particle shape. Scanning electron microscope images were recorded with a *Phenom* ProX SEM in the backscattered electron mode (BSE). TEM images were recorded with a *FEI* Titan 80-300

Journal : 10853 - Large 10853 Dispatch : 20-9-2017 Pages : 11
Article No. : 1609 ☐ LE ☐ TYPESET
MS Code : JMSC-D-17-04034 ☑ CP ☑ DISK

operating with an electron energy of 300 kV. Temperature-dependent magnetic moments were measured in the temperature range 3–300 K under field-cooled (FC) and zero-field-cooled (ZFC) conditions using a *Quantum Design* PPMS 9. An Impedance Analyzer 4192A (Hewlett Packard) was used for permittivity measurements up to 10 MHz. Gold electrodes were sputtered onto the ceramic bodies in a *Cressington* Sputter Coater 108auto. Diffuse reflectance spectra were recorded at room temperature using a *Perkin Elmer* UV–Vis spectrometer Lambda 19 with $BaSO_4$ as white standard.

Results and discussion

Synthesis and powder characterization

Calcination of the viscous (Ba,Fe,Nb)-gel in static air at 250 °C for 0.5 h resulted in a black–brown amorphous powder. Simultaneous TG/DTA measurements up to 1000 °C with a heating rate of 10 K min^{-1} in flowing air were carried out on this powder (Fig. 1). The sample shows a continuously weight loss of 6.7% up to 195 °C in combination with a very weak and broad endothermic signal, which is probably due to the release of absorbed molecules, such as H_2O. At higher temperatures, a two-step decomposition process, accompanied by exothermic signals, occurs. The first step results in a weight loss of 48.8% at 390 °C, and the second step leads to a loss of 81.1% up to 445 °C. The DTA shows a first weak exothermic signal with an onset temperature of 250 °C and a very strong second one with an onset temperature of 395 °C. This strong exothermic reaction can be assigned to a combustion-like reaction in which the organic components (mainly glucose and citric acid) act as fuel and the nitrate ions as oxidizing agent. Between 445 and 530 °C, a last very small weight change can be observed, resulting in a total weight loss of 84.5%. The dark brown residue was identified as $BaFe_{0.5}Nb_{0.5}O_3$ by XRD measurement.

The phase evolution during the thermal decomposition of the (Ba,Fe,Nb)-gel is shown in Fig. 2. For these investigations, aliquots of the gel were heated in static air in a muffle furnace at different temperatures for 2 h (rate 10 K min^{-1}). Up to 500 °C, the calcination process results in amorphous compounds. After calcination at 600 °C, first reflections of $BaFe_{0.5}Nb_{0.5}O_3$ are visible (Fig. 2a). Calcination at 800 °C leads to well-pronounced $BaFe_{0.5}Nb_{0.5}O_3$ peaks, but very small traces of a secondary phase (not clearly assignable) are detectable (Fig. 2b). Heating at 900 °C (Fig. 2c) leads to a phase-pure brown powder. No peak splitting or asymmetric broadening was found in the XRD pattern, indicating the formation of cubic $BaFe_{0.5}Nb_{0.5}O_3$ (JCPDS 01-074-6520). The crystallite size increases from 27 nm after calcination at 850 °C to 83 nm at 1100 °C (rate 10 K min^{-1}), whereas the strain parameter decreases with temperature (Fig. 3). Decomposition with a lower heating rate of 1 K min^{-1} leads to phase-pure $BaFe_{0.5}Nb_{0.5}O_3$ even at 850 °C after 2 h (Fig. 2d).

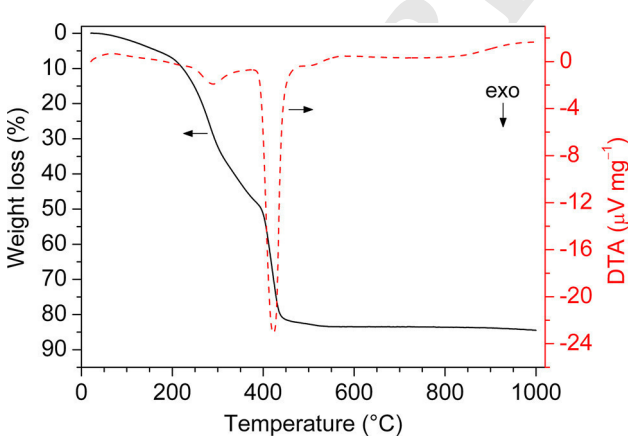

Figure 1 TG-DTA measurements of a preheated (Ba,Fe,Nb)-gel in flowing air (heating rate 10 K min^{-1}).

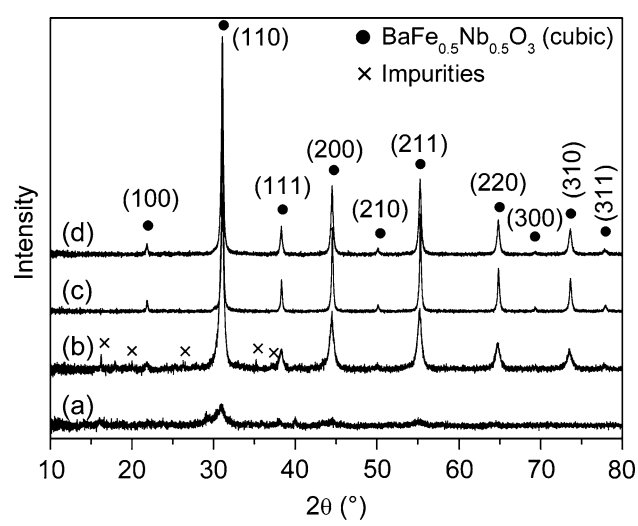

Figure 2 Room-temperature XRD patterns of the (Ba,Fe,Nb)-gel after calcination at various temperatures for 2 h: **a** 600 °C, **b** 800 °C, **c** 900 °C (heating rate 10 K min^{-1}), and **d** 850 °C (heating rate 1 K min^{-1}).

Journal : 10853 - Large 10853 | Dispatch : 20-9-2017 | Pages : 11
Article No. : 1609 | LE | TYPESET
MS Code : JMSC-D-17-04034 | CP | DISK

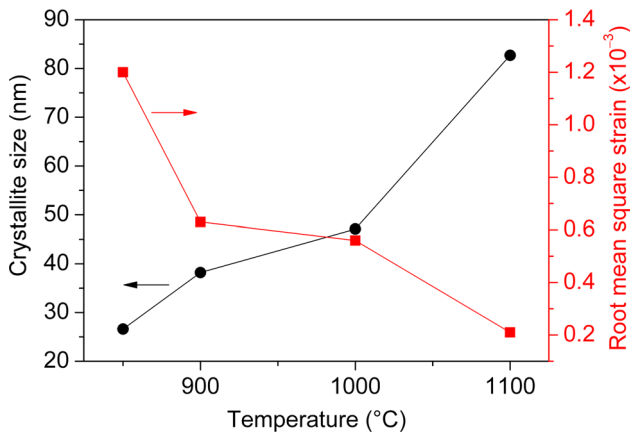

Figrue 3 Dependence of volume-weighted average crystallite size and root-mean-square strain on the calcination temperature (heating rate 10 K min^{-1}).

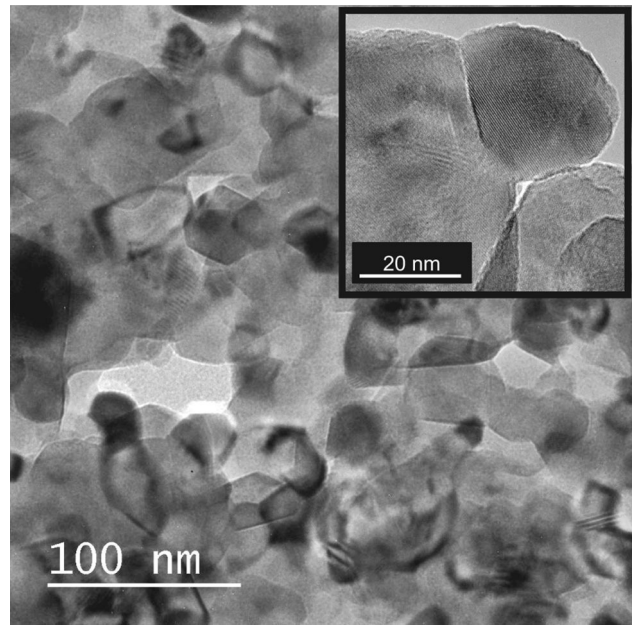

Figrue 4 TEM image of $BaFe_{0.5}Nb_{0.5}O_3$ powder calcined at 850 °C for 2 h (heating rate 1 K min^{-1}).

The addition of glucose during the synthesis process results in a reduction in the crystallite size after thermal decomposition. For example, a crystallite size of 47 nm was obtained after decomposition at 1000 °C for 2 h, while the identical synthesis route without glucose led to a crystallite size of 63 nm. The decrease in crystallite size by adding glucose is probably due to the increased fuel (organic molecules)-to-oxidizer (nitrate ions) ratio, which leads to a reduction in the maximum combustion temperature [32, 33].

Sintering behaviour and microstructure of ceramic bodies

To investigate the sintering behaviour and to obtain ceramic bodies, the (Ba,Fe,Nb)-gel was calcined at 850 °C for 2 h with a heating rate of 1 K min^{-1}. This thermal treatment leads to a phase-pure nano-crystalline $BaFe_{0.5}Nb_{0.5}O_3$ powder with a volume-weighted average crystallite size of 28 nm and a root-mean-square strain of 0.0013. The specific surface area was determined as 6.91 m^2 g^{-1} which corresponds to a calculated equivalent particle size of 134 nm. The large difference between the crystallite size and the particle size from BET measurement can be explained assuming strong agglomeration and in turn surface areas unavailable for nitrogen adsorption. TEM images support this interpretation as they show agglomerates consisting of particles with diameters between about 20 and 45 nm (Fig. 4). The present synthesis method leads to a considerable reduction in the calcining temperature and time to form single-phase $BaFe_{0.5}Nb_{0.5}O_3$ powders compared to the classical mixed-oxide method as well as to other sol–gel and co-precipitate routes [10, 13, 17, 22, 27].

A non-isothermal dilatometric measurement (up to 1500 °C) on a powder compact in flowing air shows that the shrinkage process starts at about 900 °C (Fig. 5). A first shrinkage process shows a broad maximum of the shrinkage rate of around − 0.5% min^{-1} between 990 and 1040 °C. This first step is completed at 1225 °C and results in a shrinkage of 23% (81% of the total shrinkage). Between 1225 and 1240 °C, a narrow plateau occurs. According to investigations by Hirata et al. [34], this plateau reflects grain growth processes within agglomerates without dwindling of pores. A similar behaviour was also observed for nano-sized $MgFe_2O_4$ [35]. A second shrinking process starts at about 1240 °C and shows a maximum shrinkage rate of − 0.23% min^{-1} at 1323 °C. Between 1385 and 1400 °C, a very weak expansion of the sample of 0.4% can be observed. The reason for this small expansion process is not yet clear although it was reproduced in several experiments. The whole shrinkage process is finished at 1450 °C.

The final bulk densities of ceramic bodies after conventional isothermal sintering for 1 h in static air (heating/cooling rate 5 K min^{-1}) is shown in Fig. 6. The absolute bulk densities of the sintered bodies were calculated from their weight and geometric

Journal : 10853 - Large 10853 Dispatch : 20-9-2017 Pages : 11
Article No. : 1609 ☐ LE ☐ TYPESET
MS Code : JMSC-D-17-04034 ☑ CP ☑ DISK

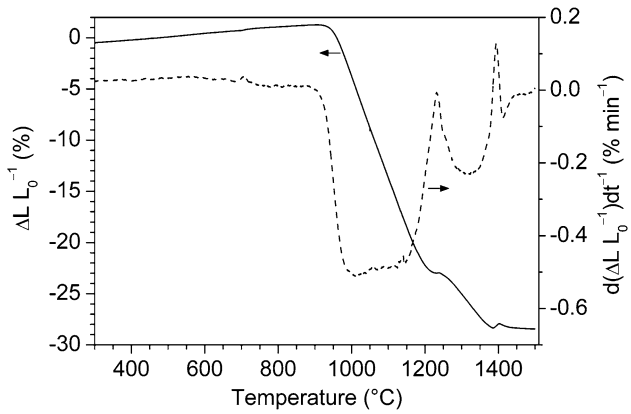

Figure 5 Non-isothermal dilatometric measurement up to 1500 °C (heating rate 5 K min^{-1}) of a compacted powder (calcined at 850 °C for 2 h).

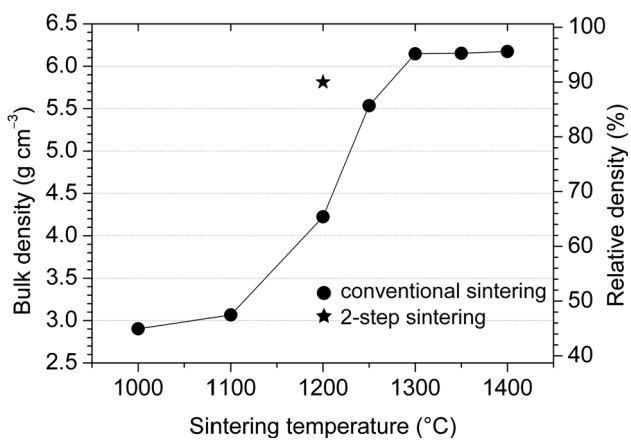

Figure 6 Final bulk densities versus sintering temperature of ceramic bodies after conventional sintering for 1 h and a two-step sintering procedure.

dimensions, and the relative bulk densities are related to the single crystal density of 6.46 g cm^{-3} [15]. We obtained dense ceramics (relative density ≥ 90%) after 1-h sintering above 1250 °C. Sintering at 1300 °C results in a relative density of 95% which remains almost constant at higher temperatures. For comparison, dense ceramic bodies of $BaFe_{0.5}Nb_{0.5}O_3$ via a classical mixed-oxide route can be obtained after sintering at a minimum temperature of 1350 °C and soaking times more than 1 h [17, 27, 36].

SEM images of selected ceramic bodies are depicted in Fig. 7. As can be seen, very compact microstructures were obtained and only few pores can be found in accordance with the high densities. The average grain size ($\varnothing_{li}$) was determined by the lineal intercept method [37]. One-hour sintering at 1200 °C results in very small grains between 0.18 and 0.60 μm ($\varnothing_{li}$ = 0.33 μm). Raising the temperature to 1250 °C, the grain size ranges between 0.5 and 3.5 μm ($\varnothing_{li}$ = 1.9 μm), while after sintering at 1350 °C the ceramic consists of grains between 7 and 34 μm ($\varnothing_{li}$ = 19.9 μm). Additional values for further sintering temperatures are listed in Table 1.

To enhance the densification at lower temperatures, a two-step sintering regime was used. A compacted powder was first heated rapidly (20 K min^{-1}) to 1300 °C (T_1), then fast-cooled (20 K min^{-1}) to 1200 °C (T_2), and held at T_2 for 10 h (see inset in Fig. 6). The resulting ceramic body had a relative bulk density of 90% and consisted of grains between 0.75 and 4.2 μm ($\varnothing_{li}$ = 2.3 μm). The sintering temperatures are reduced by 200 °C compared to the two-step sintering process of a nano-powder from a co-precipitation method reported by Wang et al. [27].

XRD patterns of the powdered ceramic bodies sintered up to 1400 °C show only reflections of cubic $BaFe_{0.5}Nb_{0.5}O_3$, without any indications for impurities (Fig. S1, supported information). In contrast to the sol–gel synthesis described by Patel et al. [5], we did not observe the formation of secondary phases even at high sintering temperatures above 1250 °C. Additionally, our XRD patterns did not reveal any superlattice peaks, indicating a random distribution of iron and niobium ions in contrast to investigations by Tezuka et al. [14]. Therefore, the XRD pattern of the sample sintered at 1350 °C was refined on the basis of the cubic perovskite structure (SG $Pm\bar{3}m$, no. 221). The lattice parameter was calculated as a = 406.11(1) pm (see also Fig. S2, supported information), close to the value found by Galasso and Darby [15].

UV–Vis, magnetic, and dielectric measurements

The diffuse reflectance spectra of $BaFe_{0.5}Nb_{0.5}O_6$ powder calcined at 850 °C for 2 h are shown in Fig. 8. The *Kubelka–Munk* theory was used for determining the optical band gap [38, 39]. The best fit to a straight line near the absorption edge was obtained assuming a direct allowed transition in accordance with literature [40]. Thus, the optical band gap (E_g) can be determined by plotting $(F(R) \cdot h\nu)^2$ versus $h\nu$ ($F(R)$ = Kubelka–Munk function) and extrapolating the slope to $F(R) \rightarrow 0$ (inset I in Fig. 8) [41]. The optical band gap of the pre-ceramic powder, calcined at 850 °

Journal : 10853 - Large 10853 Dispatch : 20-9-2017 Pages : 11
Article No. : 1609 LE TYPESET
MS Code : JMSC-D-17-04034 CP DISK

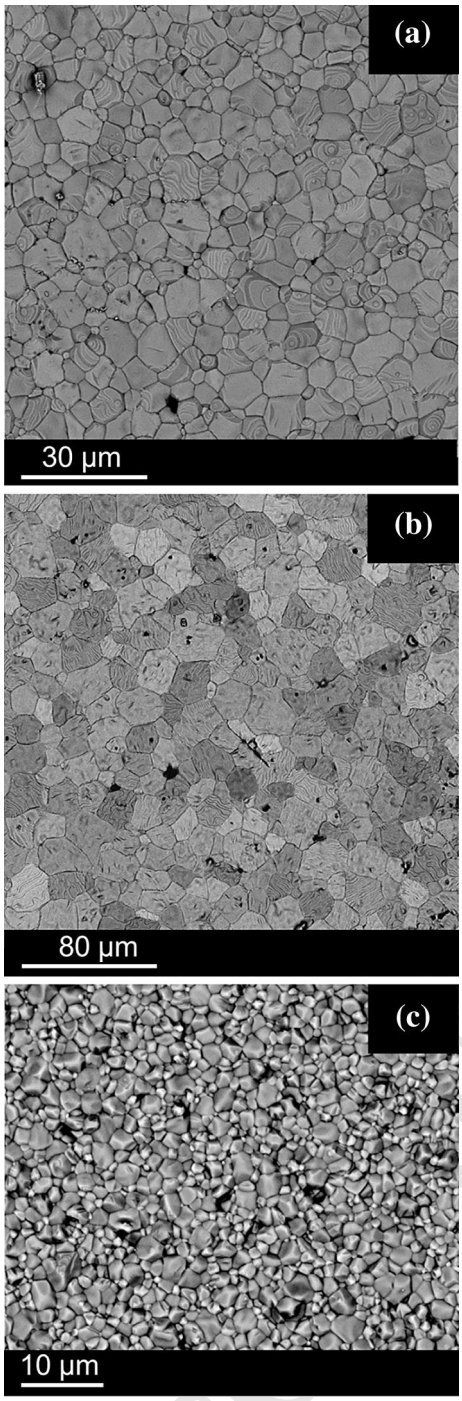

Figrue 7 SEM-BSE surface images of selected ceramic bodies conventionally sintered at **a** 1300 °C/1 h, **b** 1350 °C/1 h, and **c** two-step sintering at T_2 = 1200 °C/10 h.

C for 2 h, was calculated as 2.75(4) eV. This value decreased after sintering (inset II in Fig. 8). After 1-h heating at 1000 °C, the ceramics revealed a band gap of 2.68(4) eV which is further reduced to 2.59(2) eV after heating at 1200 °C but does not change significantly for higher sintering temperatures (e.g. 2.62 (2) eV after 1400 °C). The obtained optical band gap values are in the range reported by Patel et al. [40], whereas Kar et al. [42] surprisingly reported a much smaller band gap of only 1.3 eV.

$BaFe_{0.5}Nb_{0.5}O_3$ is an antiferromagnet with a Néel temperature (T_N) of about 25 K [14]. Figure 9 shows exemplarily the ZFC and FC curves of a ceramic body conventionally sintered at 1350 °C for 1 h. Below T_N, the ZFC curve reveals a reduced magnetic moment, whereas the FC curve only shows a kink at T_N. The Néel temperature depends slightly on the sintering temperature (inset I in Fig. 9). After sintering at 1000 °C, T_N is 19 K, rises to 23 K after sintering at 1300 °C and remains constant at higher sintering temperatures. Our values of $T_N \approx 23$ K are close to values reported in Refs. [14, 26]. Field dependent measurements at 300 K reveal a very weak spontaneous magnetization indicated by a hysteresis loop (inset II in Fig. 9). This weak spontaneous magnetization found in all ceramic bodies might be due to the presence of marginal traces of ferrimagnetic $BaFe_{12}O_{19}$ not detectable by XRD. By a linear extrapolation of the high-field region, we obtained saturation magnetizations of 0.13–0.21 emu g^{-1} in different samples. Using the saturation magnetization of pure $BaFe_{12}O_{19}$ (M_s = 57–66 emu g^{-1} [43, 44]), these values correspond to a weight proportion of 0.20–0.37% in our samples. Trace impurities of $MFe_{12}O_{16}$ have already been proposed as the origin of weak spontaneous magnetization at room temperatures in related systems like $PbFe_{0.5}Nb_{0.5}O_3$– and $PbFe_{0.5}Ta_{0.5}O_3$ ceramics [45–47]. On the other hand, even with very long counting times (10 s per data point) our XRD patterns of ceramic bodies showed no peaks corresponding to secondary phases. Still, such low contents as mentioned above might be below the detection limit even of modern diffractometers. Longer soaking times were found to lead to a reduction of the weak spontaneous magnetization corresponding to calculated $BaFe_{12}O_{19}$ contents of about 0.17 and 0.14 wt % after soaking times of 25 and 50 h at 1350 °C, respectively. As a result, the reported ferromagnetic behaviour and large magnetic moments for some $BaFe_{0.5}Nb_{0.5}O_3$ samples [23, 29] are due to such ferrimagnetic impurities.

Frequency-dependent dielectric measurements at room temperature (22 °C) between 0.1 kHz and 10 MHz of ceramics are shown in Fig. 10. Applying

Journal : 10853 - Large 10853 Dispatch : 20-9-2017 Pages : 11
Article No. : 1609 ☐ LE ☐ TYPESET
MS Code : JMSC-D-17-04034 ☑ CP ☑ DISK

Table 1 Grain sizes and dielectric values of selected ceramic bodies

Sintering regime	Average grain size[a] (grain size range)	ε_r^d	tan δ[d]
Conventional sintering[b]			
1200 °C, 1 h	0.33 μm (0.18–0.6 μm)		
1250 °C, 1 h	1.9 μm (0.5–3.5 μm)	9540	0.26
1300 °C, 1 h	8.8 μm (1.5–14 μm)	59420	0.77
1350 °C, 1 h	19.9 μm (7–34 μm)	106480	0.88
1400 °C, 1 h	51.8 μm (15–84 μm)		
Two-step sintering[c]			
T_1 = 1300 °C, T_2 = 1200 °C, 10 h	2.3 μm (0.75–4.2 μm)	28580	0.72

[a] Lineal intercept method

[b] Temperature rate 5 K min^{-1}

[c] Temperature rate 20 K min^{-1}

[d] 22 °C, 1 kHz

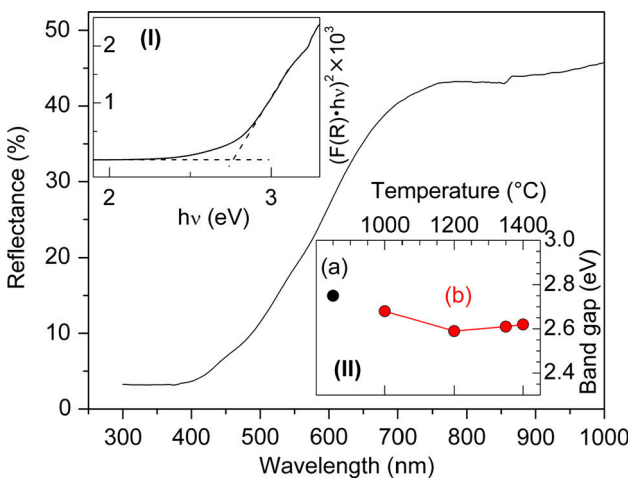

Figure 8 Diffuse reflectance spectra of the nano-powder calcined at 850 °C for 2 h. Inset (I) shows $(F(R)\cdot h\nu)^2$ versus hν. Inset (II) shows the band gap energy versus thermal treatment of **a** calcined powder at 850 °C and **b** sintered ceramics.

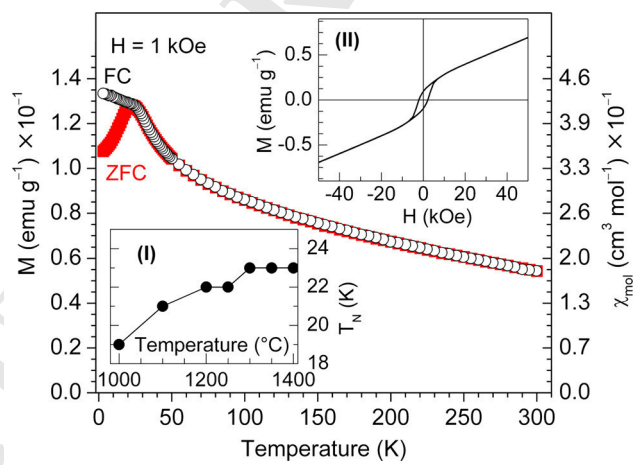

Figure 9 Temperature dependence (3–300 K) of the magnetization under zero-field-cooled (ZFC) and field-cooled (FC) conditions demonstrated for a ceramic sintered at 1350 °C for 1 h. Inset (I) shows the Néel temperature (T_N) versus sintering temperature (soaking time 1 h), and inset (II) shows the field-dependent magnetization at 300 K.

the model of a lossy capacitor, the ceramics show decreasing relative permittivities (ε_r) with increasing frequency. Up to a sintering temperature of 1350 °C, the relative permittivities increase with sintering temperature (Table 1). The values range between 9.5×10^3 and 10.6×10^4, and the tan δ values vary from 0.26 to 0.88 at 1 kHz. At frequencies above 100 kHz, the permittivity values of the conventionally sintered ceramics decrease drastically; however, the two-step sintered ceramic shows higher permittivity values. Above 10 kHz, the loss tangent increases and reaches a maximum at about 1 MHz for conventionally sintered ceramics and at 2 MHz for the two-step sintered one. The general trend of a strong decrease in the relative permittivity and a corresponding maximum of tan δ is often found in $BaFe_{0.5}Nb_{0.5}O_3$ ceramics [17, 27, 42].

The temperature dependence of the relative permittivity and the dissipation factor at 1 kHz is shown in Fig. 11. All samples show rising permittivity and tan δ values with temperature. Between 25 and 190 °C, the sample sintered at 1350 °C shows the highest permittivity values of 10.7×10^4 to 46.2×10^4 and tan δ values in the range of 0.48 and 1.83. On the other hand, the ceramic sintered at 1300 °C shows the lowest dissipation factor at higher temperatures along with the lowest temperature dependency of tan δ. Compared to samples prepared by the mixed-

Journal : 10853 - Large 10853 Dispatch : 20-9-2017 Pages : 11
Article No. : 1609 LE TYPESET
MS Code : JMSC-D-17-04034 CP DISK

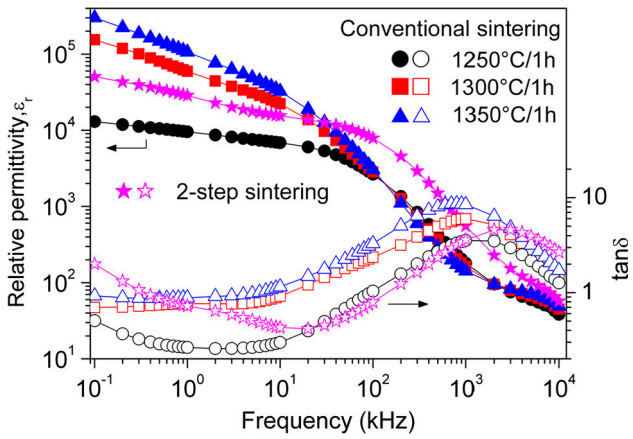

Figure 10 Dependence of the real part of the relative permittivity (closed symbols) and the dissipation factor (open symbols) on the frequency at 22 °C for ceramic bodies sintered at the indicated temperatures.

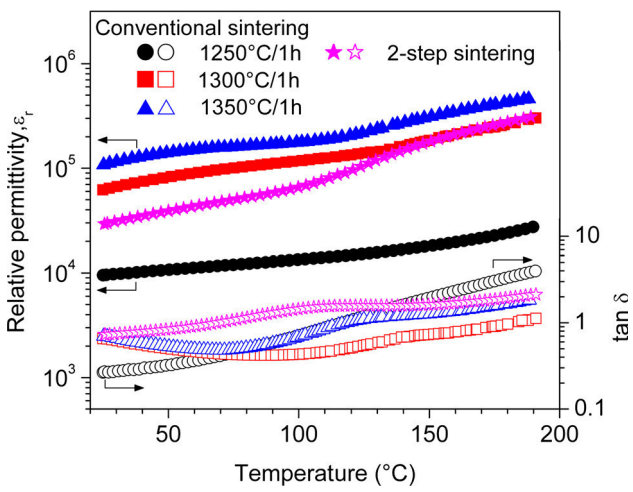

Figure 11 Temperature dependence of ε_r (closed symbols) and tan δ (open symbols) at 1 kHz for ceramic bodies sintered at the indicated temperatures.

oxide method [9, 16, 24, 48] and a sol–gel route [5], the ceramics described herein show up to one order of magnitude higher permittivity values reaching 10.6×10^4 at 1 kHz and moderate tan δ values (< 1) at room temperature.

The above discussion does not consider a possible dc-conductivity, which may be the origin of such high dielectric loss values. For a deeper understanding of the impedance data, the electrical properties therefore were modelled using a circuit of a resistance and capacitor connected in parallel (RC-element). The complex impedance (ρ^*) is described by:

$$\rho^* = \frac{\rho_{dc}}{1 + (i\omega\tau)^{\beta}} \quad (1)$$

where β is the constant phase shift (CPE) coefficient and $\tau = \rho_{dc}\varepsilon\varepsilon_0$. Details of this approach have been reported elsewhere [49]. As an example, Fig. 12 depicts the frequency dependence of the real (ρ′) and imaginary (ρ″) parts of the specific impedance at room temperature for a ceramic body conventionally sintered at 1250 °C. The Cole–Cole plots reveal single semicircular arcs (Fig. S3, supported information) up to a temperature of 190 °C, proving that the impedance data of all ceramic samples can be well described by an equivalent circuit consisting of a single RC-element. From the fits, the calculated relative permittivities at room temperature of dense ceramics conventionally sintered at 1250, 1300, and 1350 °C are $2.09(2) \times 10^4$, $73(4) \times 10^4$, and $120(1) \times 10^4$, respectively. Simultaneously, the dc-resistivity (ρ_{dc}) decreases with rising sintering temperature from 4420(13) and 1330(19), to 277(5) kΩ cm. For the two-step sintered ceramic, values of $\varepsilon = 4.83(4) \times 10^4$ and $\rho_{dc} = 219(5)$ kΩ cm were found. The activation energy (E_A) of the resistivity (ρ_{dc}) for the ceramic body sintered at 1250 °C was calculated as 0.39(3) eV using an Arrhenius plot (inset in Fig. 12). The activation energy is somewhat higher than that recently found for $BaFe_{0.5}Nb_{0.5}O_3$ samples prepared by a solution precipitation route [27]. Such a comparatively low activation energy ($E_A \ll E_g/2$) points

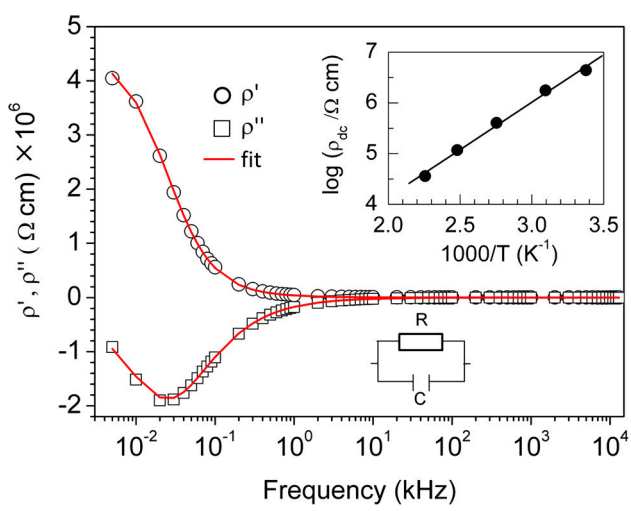

Figure 12 Dependence of the real and imaginary parts of the specific impedance (ρ′, ρ″) on the frequency at 22 °C for a ceramic body conventionally sintered at 1250 °C for 1 h. The inset shows the Arrhenius plot of log ρ_{dc} versus 1000/T.

Journal : 10853 - Large 10853 | Dispatch : 20-9-2017 | Pages : 11
Article No. : 1609 | LE | TYPESET
MS Code : JMSC-D-17-04034 | CP | DISK

to defects possibly due to oxygen vacancies and in turn partial reduction of Fe^{3+} and Nb^{5+}. Additionally, the ceramics show a decrease in the dc-resistivity with rising measurement temperature, indicating a semiconductor-like behaviour.

Conclusion

A nano-crystalline $BaFe_{0.5}Nb_{0.5}O_3$ powder with an enhanced sintering activity was synthesized by a modified Pechini-like polymerization route using glucose as additional component. The obtained (Ba, Fe,Nb)-gel was calcined at 850 °C (rate 1 K min^{-1}) to yield phase-pure $BaFe_{0.5}Nb_{0.5}O_3$ with a crystallite size of 28 nm. Because of the nano-crystalline nature of this powder, dense ceramic bodies with variable grain sizes and different dielectric characteristics can be obtained. Dense ceramic bodies (relative density ≥ 90%) can be obtained after conventional sintering above 1250 °C for 1 h or after a two-step sintering procedure at 1200 °C. The optical band gap of the nano-powder is 2.75(4) eV and slightly decreases upon sintering to 2.59(2) eV. Magnetic measurements show a Néel temperature of about 23 K for the dense ceramic bodies. Dielectric measurements were carried out depending on frequency and temperature. The highest permittivity values at 1 kHz of 10.6×10^4 were reached after sintering at 1350 °C for 1 h. The tan δ values show a maximum at 1–2 MHz with values between 4.6 and 8.6 at RT. The impedance data can be fitted assuming an equivalent circuit with one RC-element. The synthesis route described in this article leads to phase-pure $BaFe_{0.5}Nb_{0.5}O_3$ powder at lower calcining temperature and time compared to other synthesis routes. The resulting nano-grained powder compacts show a reduction in the sintering temperature up to 200 °C, and the ceramic bodies show much higher permittivity and moderate loss tangent values compared to conventional syntheses.

Acknowledgements

We are grateful to Dr. E. Pippel (Max Planck Institute of Microstructure Physics, Halle/Saale) for the TEM images. Financial support by the German Research Foundation within the Collaborative Research Centre (SFB 762) *Functionality of Oxide Interfaces* is gratefully acknowledged.

Compliance with ethical standards

Conflict of interest The authors declare that they have no conflict of interest.

Electronic supplementary material: The online version of this article (doi:10.1007/s10853-017-1609-1) contains supplementary material, which is available to authorized users.

References

[1] Homes CC, Vogt T, Shapiro SM, Wakimoto S, Ramirez AP (2001) Optical response of high-dielectric-constant perovskite-related oxide. Science 293:673–676

[2] Chung SY, Kim ID, Kang SJ (2004) Strong nonlinear current–voltage behaviour in perovskite-derivative calcium copper titanate. Nat Mater 3:774–778

[3] Haertling GH (1999) Ferroelectric ceramics: history and technology. J Am Ceram Soc 82:797–818

[4] Ke S, Fan H, Huang H (2009) Dielectric relaxation in A_2FeNbO_6 (A = Ba, Sr, and Ca) perovskite ceramics. J Electroceram 22:252–256

[5] Patel PK, Yadav KL, Singh H, Yadav AK (2014) Origin of giant dielectric constant and magnetodielectric study in Ba$(Fe_{0.5}Nb_{0.5})O_3$ nanoceramics. J Alloys Compd 591:224–229

[6] Wang Z, Chen XM, Ni L, Liu XQ (2007) Dielectric abnormities of complex perovskite $Ba(Fe_{1/2}Nb_{1/2})O_3$ ceramics over broad temperature and frequency range. Appl Phys Lett 90:022904

[7] Ke S, Lin P, Huang H, Fan H, Zeng X (2013) Mean-Field Approach to Dielectric Relaxation in Giant Dielectric Constant Perovskite Ceramics, J Ceram 795827 AQ1

[8] Bochenek D, Niemiec P, Szafraniak-Wiza I, Adamczyk M, Skulski R (2015) Preparation and dielectric properties of the lead-free $BaFe_{1/2}Nb_{1/2}O_3$ ceramics obtained from mechanically triggered powder. Eur Phys J B 88:277

[9] Kantha P, Pisitpipathsin N, Pengpat K, Rujijanagul G, Guo R, Bhalla AS (2011) Microstructure and electrical properties of $BaFe_{0.5}Nb_{0.5}O_3$ doped with GeO_2 (1–5 wt%). Ferroelectrics 425:27–38

[10] Charoenthai N, Traiphol R (2011) Progress in the synthesis of $Ba(Fe_{0.5}Nb_{0.5})O_3$ ceramics: a versatile co-precipitation method. J Ceram Process Res 12:191–194

[11] Raevski IP, Kuropatkina SA, Kubrin SP, Raevskaya SI, Titov VV, Sarychev DA, Malitskaya MA, Bogatin AS, Zakharchenko IN (2009) Dielectric and Mössbauer studies

Journal : 10853 - Large 10853 | Dispatch : 20-9-2017 | Pages : 11
Article No. : 1609 | LE | TYPESET
MS Code : JMSC-D-17-04034 | CP | DISK

of high-permittivity $BaFe_{1/2}Nb_{1/2}O_3$ ceramics with cubic and monoclinic perovskite structures. Ferroelectrics 379:48–54

[12] Saha S, Sinha TP (2002) Low-temperature scaling behavior of $BaFe_{0.5}Nb_{0.5}O_3$. Phys Rev B 65:134103

[13] Chung CY, Chang YH, Chen GJ, Chai YL (2005) Preparation, structure and ferroelectric properties of $Ba(Fe_{0.5}Nb_{0.5})O_3$ powders by sol–gel method. J Cryst Growth 284:100–107

[14] Tezuka K, Henmi K, Hinutsa Y (2000) Magnetic susceptibilities and mössbauer spectra of perovskites A_2FeNbO_6 (A = Sr, Ba). J Solid State Chem 154:591–597

[15] Galasso F, Darby W (1962) Ordering of the octahedrally coordinated cation position in the perovskite structure. J Phys Chem 66:131–132

[16] Bhagat S, Prasad K (2010) Structural and impedance spectroscopy analysis of $Ba(Fe_{1/2}Nb_{1/2})O_3$ ceramic. Phys Status Solidi A 207:1232–1239

[17] Kar SK, Kumar P (2013) Permittivity and modulus spectroscopic study of $BaFe_{0.5}Nb_{0.5}O_3$ ceramics. Process Appl Ceram 7:181–187

[18] Kar SK, Kumar P (2013) Structural, morphological and dielectric study of $Ba(FeNb)_{0.5}O_3$ ceramics synthesized by microwave processing technique. J Phys Chem Solids 74:1408–1413

[19] Raevski IP, Prosandeev SA, Bogatin AS, Malitskaya MA, Jastrabik L (2003) High dielectric permittivity in $AFe_{1/2}B_{1/2}O_3$ nonferroelectric perovskite ceramics (A = Ba, Sr, Ca; B = Nb, Ta, Sb). J Appl Phys 93:4130–4136

[20] Voorhoeve RJH, Trimble LE, Khattak CP (1974) Extrapolation of perovskite-like catalysts: Ba_2CoWO_6 and Ba_2FeNbO_3 in NO reduction and CO oxidation. Mater Res Bull 9:655–666

[21] Chung WC, Pan KL, Lee HM, Chang MB (2014) Dry reforming of methane with dielectric barrier discharge and ferroelectric packed-bed reactors. Energy Fuels 28:7621–7631

[22] Pan KL, Chung WC, Chang MB (2014) Dry reforming of CH_4 with CO_2 to generate syngas by combined plasma catalysis. IEEE Trans Plasma Sci 42:3809–3818

[23] Rama N, Phillip JB, Opel M, Chandrasekaran K, Sankaranarayanan V, Gross R, Rao MSR (2004) Study of magnetic properties of A2B´NbO6 (A = Ba, Sr, BaSr; and B´ = Fe and Mn) double perovskites. J Appl Phys 95:7528–7530

[24] Intatha U, Eitssayeam S, Tunkasiri T (2008) Giant dielectric behavior of $BaFe_{0.5}Nb_{0.5}O_3$ perovskite ceramic. Int J Mod Phys 22:4717–4723

[25] Sun XH, Wang CC, Wang GJ, Lei CM, Li T, Mei JY, Cui YM (2012) Relationship between the dielectric properties and the conductivity of Ba_2FeNbO_6. J Electroceram 29:187–191

[26] Battle PD, Gibb TC, Herod AJ, Kim SH, Munns PH (1995) Investigation of magnetic frustration in A2FeMO6, (A = Ca, Sr, Ba; M = Nb, Ta, Sb) by magnetometry and mossbauer spectroscopy. J Mater Chem 5:865–870

[27] Wang Z, Wen YF, Li HJ, Fang MR, Wang C, Pu YP (2016) Excellent stability and low dielectric loss of $Ba(Fe_{0.5}Nb_{0.5})O_3$ synthesized by a solution precipitation method. J Alloys Compd 656:431–438

[28] Charoenthai N, Traiphol R, Rujijanagul G (2008) Microwave synthesis of barium iron niobate and dielectric properties. Mater Lett 62:4446–4448

[29] Jha AK, Prasad K (2014) Green synthesis and characterization of $BaFe_{0.5}Nb_{0.5}O_3$ nanoparticles. J Chin Adv Mater Sci 2:294–302

[30] Program WinXPOW v2.11, Stoe & Cie GmbH, Darmstadt, 2004

[31] Rodriguez-Carvajal J (1993) Recent advances in magnetic structure determination neutron powder diffraction. Phys B 192:55–69

[32] Köferstein R (2014) Synthesis, phase evolution and properties of phase-pure nanocrystalline $BiFeO_3$ prepared by a starch-based combustion method. J Alloys Compd 590:324–330

[33] Deshpande K, Mukasyan A, Varma A (2004) Direct synthesis of iron oxide nanopowders by the combustion approach: reaction mechanism and properties. Chem Mater 16:4896–4904

[34] Hirata Y, Hara A, Aksay IA (2009) Thermodynamics of densification of powder compact. Ceram Int 35:2667–2674

[35] Köferstein R, Walther T, Hesse D, Ebbinghaus SG (2013) Preparation and characterization of nanosized magnesium ferrite powders by a starch-gel process and corresponding ceramics. J Mater Sci 48:6509–6518. doi:10.1007/s10853-013-7447-x

[36] Eitssayeam S, Intatha U, Pengpat K, Tunkasiri T (2006) Preparation and characterization of barium iron niobate ($BaFe_{0.5}Nb_{0.5}O_3$) ceramics. Curr Appl Phys 6:316–318

[37] Mendelson MI (1969) Average grain size in polycrystalline ceramics. J Am Ceram Soc 52:443–446

[38] Kubelka P, Munk F (1931) Ein beitrag zur optik der farbanstriche. Z Techn Phys 11:593–601

[39] Kortüm G, Vogel J (1958) Die Theorie der diffusen Reflexion von Licht an pulverförmigen Stoffen. Z Phys Chem 18:110–122

[40] Patel PK, Yadav KL, Kaur G (2014) Reduced dielectric loss in $Ba_{0.95}Sr_{0.05}(Fe_{0.5}Nb_{0.5})O_3$ thin film grown by pulsed laser deposition. RSC Adv 4:28056–28061

[41] Köferstein R, Buttlar T, Ebbinghaus SG (2014) Investigations on $Bi_{25}FeO_{40}$ powders synthesized by hydrothermal

Journal : 10853 - Large 10853 | Dispatch : 20-9-2017 | Pages : 11
Article No. : 1609 | ☐ LE | ☐ TYPESET
MS Code : JMSC-D-17-04034 | ☑ CP | ☑ DISK

and combustion-like processes. J Solid State Chem 217:50–56

[42] Kar SK, Swain S, Kumar P (2015) High dielectric constant and low optical band gap studies of La-modified $Ba(Fe_{0.5}Nb_{0.5})O_3$ ceramics. Mater Chem Phys 155:171–177

[43] Yu J, Tang S, Zhai L, Shi Y, Du Y (2009) Synthesis and magnetic properties of single-crystalline $BaFe_{12}O_{19}$ nanoparticles. Phys B 404:4253–4256

[44] Shafie MSE, Hashim M, Ismail I, Kanagesan S, Fadzidah MI, Idza IR, Hajalilou A, Sabbaghizadeh R (2014) Magnetic M-H loops family characteristics in the microstructure evolution of BaFe12O19. J Mater Sci Mater Electron 25:3787–3794

[45] Raevski IP, Titov VV, Malitskaya MA, Eremin EV, Kubrin SP, Blazhevich AV, Chen H, Chou CC, Raevskaya SI, Zakharchenko IN, Sarychev DA, Shevtsova SI (2014) Studies of ferroelectric and magnetic phase transitions in multiferroic $PbFe_{0.5}Ta_{0.5}O_3$–$PbTiO_3$ solid solution ceramics. J Mater Sci 49:6459–6466. doi:10.1080/00150193.2015.995009

[46] Puri M, Bahel S, Raevski IP, Narang SB (2016) Structural, dielectric and magnetic properties of $(Pb_{1-x}Ca_x)(Fe_{0.5}Nb_{0.5})O_3$ solid solution ceramics. J Magnet Magnet Mater 407:195–200

[47] Amonpattaratkit P, Jantaratana P, Ananta S (2015) Influences of PZT addition on phase formation and magnetic properties of perovskite $Pb(Fe_{0.5}Nb_{0.5})O_3$-based ceramics. J Magnet Magnet Mater 389:95–100

[48] Intatha U, Eitssayeam S, Pengpat K, MacKenzie KJD, Tunkasiri T (2007) Dielectric properties of low temperature sintered LiF doped $BaFe_{0.5}Nb_{0.5}O_3$. Mater Lett 61:196–200

[49] Oehler F, Langhammer HT, Ebbinghaus SG (2017) Preparation and dielectric properties of $CaTaO_2N$ and $SrNbO_2N$ ceramics. J Eur Ceram Soc 37:2129–2136

Journal : 10853 - Large 10853 | Dispatch : 20-9-2017 | Pages : 11
Article No. : 1609 | ☐ LE | ☐ TYPESET
MS Code : JMSC-D-17-04034 | ☑ CP | ☑ DISK

Supporting Information

J. Mater. Sci.

Magnetic, optical, dielectric, and sintering properties of nano-crystalline $BaFe_{0.5}Nb_{0.5}O_3$ synthesized by a polymerization method

Roberto Köferstein*, Florian Oehler, and Stefan G. Ebbinghaus

Institute of Chemistry, Martin Luther University Halle-Wittenberg, Kurt-Mothes-Strasse 2, 06120 Halle, Germany.

* Corresponding author. Tel.: +49-345-5525630; Fax: +49-345-5527028.
E-mail address: roberto.koeferstein@chemie.uni-halle.de

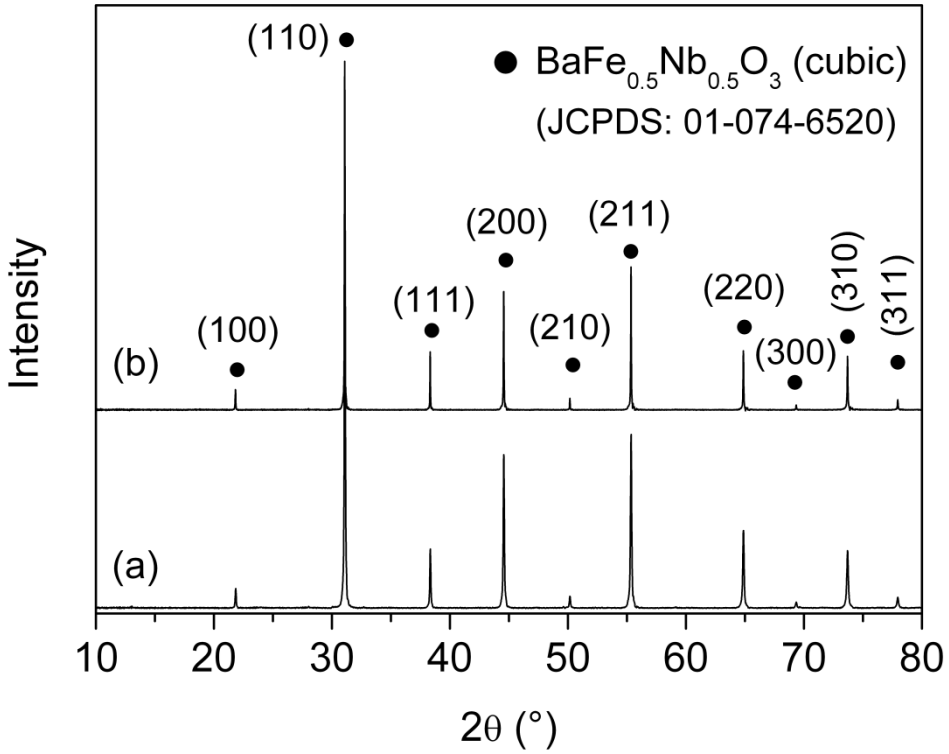

Fig. S1: XRD patterns of powdered ceramic bodies sintered (rate 5 K min^{-1}) at (a) 1000 °C, 1 h and (b) 1400 °C, 1 h.

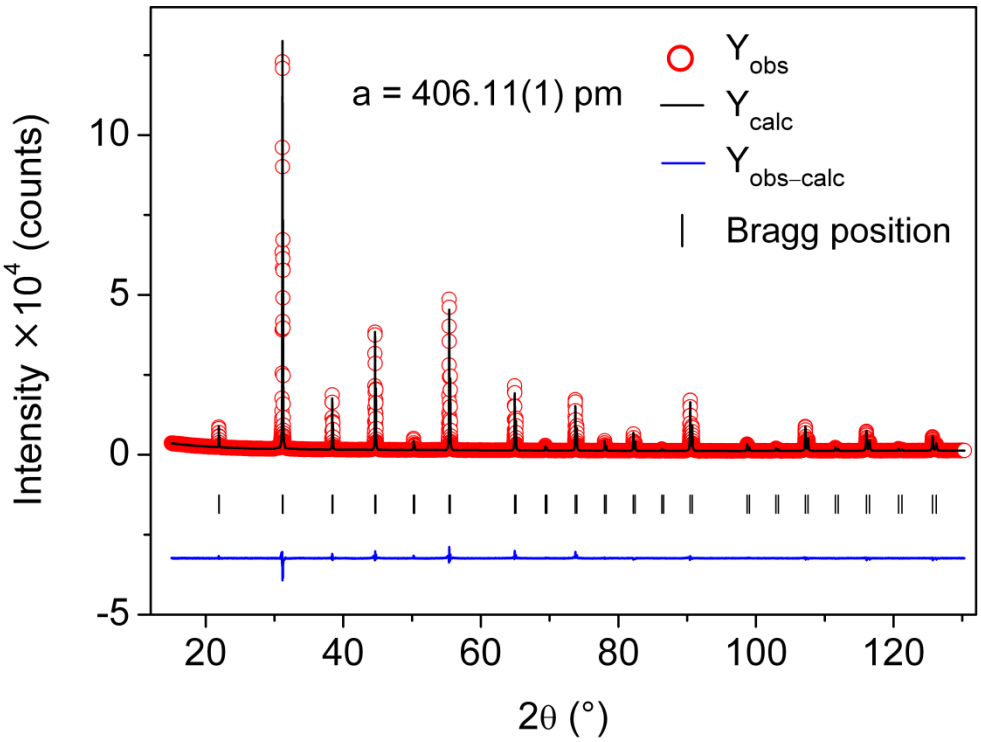

Fig. S2: Rietveld refinement (Cu-$K_{\alpha1+\alpha2}$ radiation) of a ceramic sample sintered at 1350 °C for 1 h. (R_p = 3.19%, R_{wp} = 4.46%, and χ^2 = 3.72).

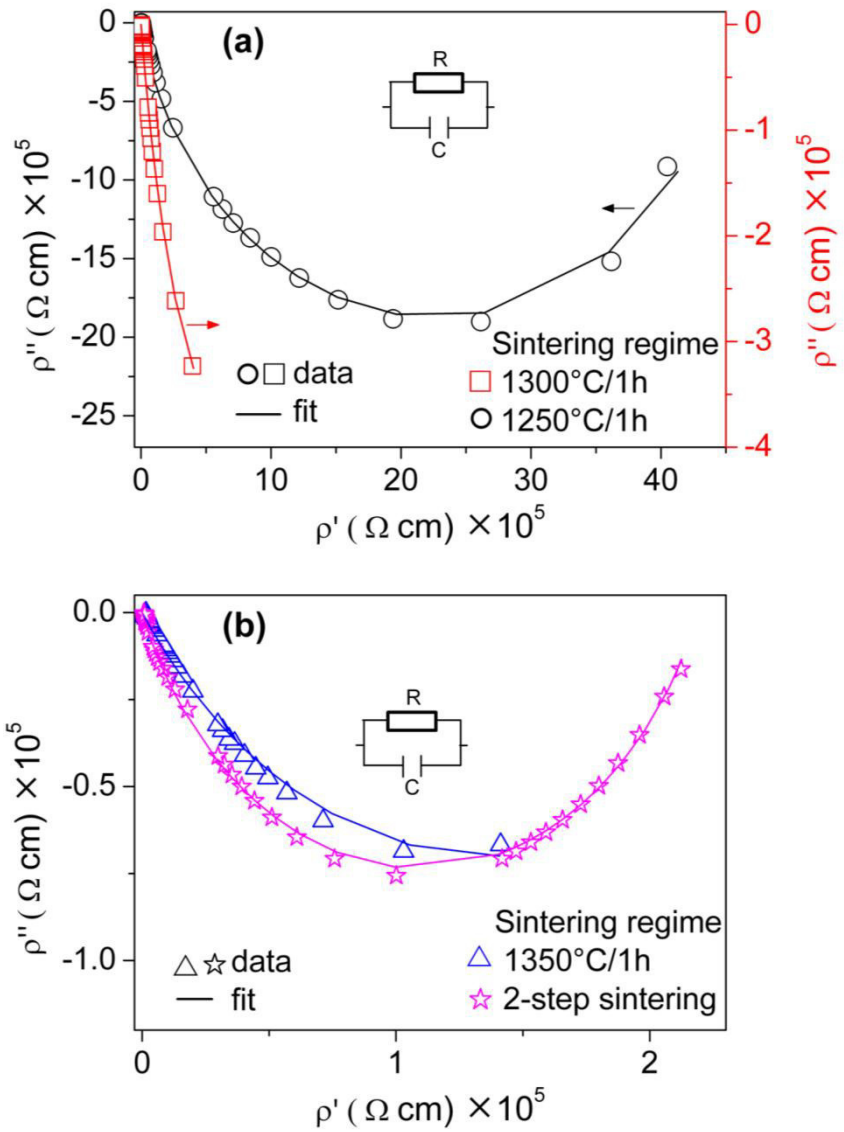

Fig. S3: Cole-Cole plots at room temperature of $BaFe_{0.5}Nb_{0.5}O_3$ ceramics sintered at the indicated regimes. The fit was carried out using the shown equivalent circuit.